Applied Catalysis B: Environment and Energy 346 (2024) 123746

Contents lists available at ScienceDirect

Applied Catalysis B: Environment and Energy

journal homepage: www.elsevier.com/locate/apcatb

Deactivation of porphyrin metal-organic framework in advanced oxidation process: Photobleaching and underlying mechanism

Yufei Shu [a], Xun Liu [a,b], Meng Zhang [a], Bei Liu [a,*], Zhongying Wang [a,*]

[a] School of Environmental Science and Engineering, Southern University of Science and Technology, Shenzhen 518055, PR China
[b] School of Environment, Harbin Institute of Technology, PR China

ARTICLE INFO

Keywords:
Advanced oxidation processes
Deactivation
Porphyrin
Metal-organic frameworks
Photobleaching

ABSTRACT

Porphyrin metal-organic frameworks (MOFs) are widely used in photocatalytic advanced oxidation processes (AOP). However, the stability and deactivation of MOFs, crucial for reusability, have been understudied compared to their catalytic activity. We investigated photobleaching in porphyrin MOFs PCN-224-M (M= H_2, Fe, Co, Cu, Zn) under visible light and H_2O_2. The MOFs exhibited crystallinity loss, ring-opening cleavage, and linker degradation. Photobleaching resulted from direct redox reactions between porphyrin sites and H_2O_2. Metal-oxo-porphyrin intermediates played a key role in the "group effect," with different functional groups affecting the photobleaching rate: PCN-224-Fe ≈ PCN-224-Co > PCN-224-H_2 > PCN-224-Cu ≈ PCN-224-Zn. This trend related to chelated metal ions' electronic structures and their propensity for metal-oxo intermediate formation, establishing a structure-stability relationship. Our study enhances understanding of deactivation mechanisms in porphyrin MOFs during AOP, aiding the design of resilient and efficient MOF catalysts for environmental applications.

1. Introduction

Photocatalytic advanced oxidation processes (AOPs) are increasingly considered as promising techniques in water treatment, due to its usage of sustainable energy resources and high efficiency [1–4]. High oxidation efficiency was achieved by generating active oxygen species (ROS) like hydroxyl radical (·OH), superoxide ($O_2^{\cdot-}$), and etc., particularly in the presence of hydrogen peroxide (H_2O_2) and other oxidants. Photocatalytic AOPs have been widely applied in pollutant removal, including dyes [5], pharmaceuticals [6], cyanotoxins [7], and various other contaminants. Advanced oxidation processes create a strong oxidative environment for catalyzing the degradation of pollutants, yet this heightened reactivity may also lead to catalyst decomposition and hinder their reusability. Therefore, alongside enhancing catalytic performance, attention to catalyst stability and transformation is crucial for the development and refinement of AOP technologies.

Metal-organic frameworks (MOFs), a class of crystalline porous materials composed of metal-containing secondary building units (SBUs) and organic molecular linkers [8–10], have received increasing attention as photocatalysts. Recently, porphyrin or porphyrin-decorated MOFs have been intensively exploited for photocatalytic AOPs due to the high-efficient producing of ROS and oxidative metal-oxo intermediates [11–13], thanks to their light-harvesting ability and active M-N_4 sites [14–18]. Various forms of porphyrin MOFs, including free-base- [19–24], cobalt- [25,26], zinc- [27], nickel- [28], manganese- [29], and ferric-porphyrin MOFs [30–34], have demonstrated the capacity to generate ROS, thereby facilitating the degradation of organic contaminants. Similar with other catalysts which are subscribed to decomposition by ROS in AOP, some investigations have also witnessed a decrease in the reusability of porphyrin MOFs, such as PCN-222(Hf) and Fe-TCPP MOF, in long-term photocatalytic AOP applications [28,33]. Meanwhile, the photodegradation of porphyrins and their derivative molecules under irradiation has been previously reported [35–39], raising concerns regarding deactivation of porphyrin MOFs in the oxidative chemical environments.

In these years, efforts have been devoted to study the processes of deactivation and the causal factors of MOF catalysts. Some studies have reported the structural transformation on crystallinity and morphology of MOFs due to thermal, water, and pH challenges, with the stability being mainly related to the metal-ligand coordination bond strength [40–43]. In addition to these crystallographic properties, the latent transformations involving the components of MOF are also possible to

* Corresponding authors.
E-mail addresses: liub@sustech.edu.cn (B. Liu), wangzy6@sustech.edu.cn (Z. Wang).

https://doi.org/10.1016/j.apcatb.2024.123746
Received 24 October 2023; Received in revised form 12 December 2023; Accepted 14 January 2024
Available online 16 January 2024

cause the deactivation [44]. For example, recent research has witnessed the structural transformation of MOF in photo-related scenario, such as the photodecarboxylation of terephthalate MOFs [45], phase transition of Co nodes in ZIF-67 [46], photo-accelerated hydrolysis of ZIF-8 [47], and the oxidation of MOFs in ozone solutions [48]. These advancements have revealed a close correlation between the deactivations of MOF catalysts in their respective application scenarios and the irreversible transformations of the components—SBUs and/or organic linkers. Nevertheless, the relationship between MOF structure and stability has not been well established. Specifically, the role of chelating metals, which is an essential functional group in a porphyrin MOF, on the deactivation behavior remains unknown. The impact of functional groups on deactivation behaviors and corresponding structure-stability relationships holds significant implications for the design of stable MOF-based catalysts.

In this study, we unveiled intriguing photochemical transformations of zirconium porphyrin MOF PCN-224-M series (where M represents H_2, Co, Cu, Fe, Zn) in an AOP scenario, wherein porphyrin MOFs catalyze the degradation of organic dye Rhodamine B (RhB) in the presence of H_2O_2. Photobleaching phenomena and deactivation of PCN-224-Ms were observed for the porphyrin MOF catalysts, which were characterized by changes in the crystallinity and linker composition. Additionally, we investigated the deactivation pathways of porphyrin linkers and elucidated the key factor leading to the photobleaching of PCN-224-M. Finally, the underlying mechanisms governing the impact of functional groups on the deactivation rates of the PCN-224-M were revealed through a combination of hypothesis-deduction methodology, experimental results and density function theory (DFT) calculations, and the structure-stability relationship was established.

2. Materials and methods

2.1. Preparation of porphyrin MOFs

All the chemicals were purchased and used directly without further purification (Text S1). The porphyrin linker 5,10,15,20-tetrakis(4-carboxyphenyl) porphyrin (H_2TCPP), and the free-base porphyrin MOF PCN-224-H_2 were synthesized using the previously reported methods [49]. Metalloporphyrin MOFs (Co(II), Fe(III), Cu(II), Zn(II)) were obtained by post-synthetic modification from PCN-224-H_2 [50]. To synthesize PCN-224-M, 60 mg of PCN-224-H_2 and 20 mL of DMF was added to a 50 mL flask, and the mixture was sonicated for 10 min and then stirred in a magnetic stirring apparatus for 20 min to obtain uniformly dispersed MOF suspension. Subsequently, 24 mg of anhydrous cobalt chloride ($CoCl_2$) was introduced, and the reaction was conducted at 100 ℃ for 24 h under N_2 protection. After cooling, the brown powder was collected by centrifugation, followed by washing with DMF and acetone consecutively for three times at room temperature. The product was further subjected to Soxhlet extraction, involving hot refluxing acetone overnight, and finally was dried under vacuum at 80 ℃ for 12 h. Detailed synthetic methods for PCN-224-Fe, PCN-224-Cu, and PCN-224-Zn can be found in Supporting information (Text S2).

2.2. Characterization

The crystallinity of PCN-224-M was determined by powder X-ray diffraction (PXRD, Rigaku Smartlab 9 kW diffractometer) operated at 45 kV, 200 mA and Cu Kα ($\lambda = 1.5406$ Å). The morphology of PCN-224-M was characterized by scanning electron microscopy (SEM, Thermo Fisher Scientific Quattro S). The light absorbance of PCN-224-M suspension and MTCPP solution released from PCN-224-M was measured by an ultraviolet-visible absorbance spectrophotometer (UV-Vis, Hitachi UH5300). The UV-Vis diffuse reflectance spectra of PCN-224-M were recorded in the range of 400–1000 nm using an ultraviolet-visible-near-infrared diffuse reflectance spectrometer (UV-Vis-NIR DLS, PerkinElmer, lambda 750 s), with $BaSO_4$ serving as the reflection standard. The Brunauer-Emmett-Teller (BET) surface area and pore distribution of PCN-224-M was determined from the N_2 adsorption isotherms, measured by a surface adsorption analyzer (Micromeritics, ASAP2020) in a liquid N_2 bath (77 K). Before the measurements, the samples of PCN-224-M were degassed at 120 ℃ for 12 h, under a pressure below 5 Pa.

2.3. Deactivation of porphyrin MOFs

To ensure the uniform dispersion of MOFs in the AOP, 30 mg of PCN-224-M was introduced into 20 mL of ultrapure water, and sonicated in a cell disruptor (JY92, Scientz Co., Ltd., 300 W) for 30 min. To examine the catalytic ability for pollutant degradation, 50 mg/L PCN-224-M was introduced into aqueous solutions containing 10 mg/L RhB, followed by the addition of 20 mmol/L H_2O_2. For the investigation of the photobleaching process of PCN-224-M in H_2O_2 solution, 20 mmol/L H_2O_2 and 50 mg/L PCN-224-M suspensions were combined in quartz vials. These vials were then wrapped by aluminum foil and agitated at 60 rpm on a mechanical shaking table at room temperature for dark condition, or were placed in a photoreactor equipped with 5 W white LED bulbs (400 nm $\leq \lambda \leq$ 800 nm, Perfect Light Co., Ltd.). For quantitative analysis, an aliquot sample (0.25 mL) was withdrawn from of the irradiating suspension at the specific interval, and the sample was introduced into 3.75 mL of NaOH solution (10 mmol/L) to decompose the MOF. The remaining porphyrin linker content in the sample was quantified using a UV-Vis photometer (UV-Vis, Hitachi UH5300) and external standard methods (Fig. S6–S10).

2.4. Mechanism analysis of the deactivation process

To verify the ROS species generated by PCN-224-M, electron paramagnetic resonance measurements (EPR, Bruker EMXplus) were performed under both dark conditions and visible light irradiation. We used spin-trapping agent, specifically 5,5-dimethyl-1-pyrroline-*N*-oxide (DMPO, 65 mmol/L) to capture·OH and $O_2^{\cdot-}$, and 4-amino-2,2,6,6-tetramethylpiperidine (TEMP, 65 mmol/L) to detect $^1O_2$. Besides, quenching experiments were performed to assess the impact of ROS on the photobleaching process. *tert*-Butanol (TBA, 100 mmol/L), *p*-benzoquinone (*p*-BQ, 1 mmol/L) and 1,3-diphenylisobenzofuran (DPBF, 1 mmol/L) were used as scavengers of·OH, $O_2^{\cdot-}$, and $^1O_2$, respectively.

To reveal the fate of porphyrin MOFs, the as-synthesized and deactivated samples were dissolved by 10 mmol/L NaOH solution. These solutions were diluted by a factor of 5 and subjected to excitation-emission matrix spectra analysis (EEM, HORIBA Scientific Aqualog). To identify oxidation intermediates and products of porphyrin linkers within PCN-224-M during the photochemical transformation process, we conducted electrospray ionization mass spectrometry (ESI-MS, Thermo Fisher Scientific Orbitrap Fusion). For the detection of intermediates, samples taken after 15 s and 300 s of reaction in dark conditions were examined. For the detection of oxidation products, we analyzed samples taken after two-hour light irradiation. In a typical pretreatment, the solid was separated by PTFE membrane with a nominal pore size of 0.22 μm (Jinteng Co., Ltd), and the membrane was then immersed in 5 mL of NaOH solution (10 mmol/L) and sonicated. Before ESI-MS tests, the sample was acidified to pH 5 and diluted by a factor of 10 with ultrapure water.

The cyclic voltammogram (CV) measurements of PCN-224-M in the presence of H_2O_2 solution were performed using an electrochemical workstation (CHI660E, Chenhua Co., Ltd.) with a three-electrode setup, in which as-prepared MOFs, Pt plate, and Ag/AgCl electrode (3.5 M) were used as working electrode, counter electrode and reference electrode, respectively. The working electrode was fabricated by using the conventional procedure: 1 mg of PCN-224-M was dispersed in 200 μL Nafion solution (0.5%) and coated onto an indium-tin oxide glassy electrode (ITO, 1.5 ×1.5 cm). After natural dryness at room temperature, the working electrode was further dried at 353 K for 0.5 h to improve the adhesion. The CV tests were carried out using a Na_2SO_4-

H_2O_2 aqueous solution (100 mmol/L and 20 mmol/L) at room temperature.

DFT calculations were performed using the Becke's three-parameter hybrid method with the Lee, Yang, and Parr gradient-corrected correlation function (B3LYP). A mixed basis set of Lanl2dz for transition metals (Fe, Co, Cu, Zn) and 6–31 G* for C, N, O, H was adopted. The optimization, zero-point energies (ZPEs), and Gibbs free energy corrections were obtained at the same level [51,52].

3. Results and discussion

3.1. Synthesis and characterizations

A series of porphyrin MOFs PCN-224-M were synthesized (Fig. 1a), including freebase (PCN-224-H_2) and metal chelated MOFs (PCN-224-Co, -Fe, -Cu, -Zn). The successful chelation of Co(II), Fe(III), Cu(II), and Zn(II) onto the porphyrin linker in PCN-224-M was confirmed by the changes in UV-Vis absorbance spectra (Fig. S1, Table S1). Specifically, the decreases in the number of the peaks corresponding to Q-band indicated an increase in the symmetry of porphyrin linkers, which was attributed to the effective chelation of the metal ions (Text S3). Multiple characterizations were conducted to validate the structural consistence of MOFs and the complete metal chelation in PCN-224-M. SEM images (Fig. 1b–e) showed that metal-chelated PCN-224-M exhibited regular cubic morphologies, consistent with that of PCN-224-H_2 (Fig. S2). N_2 adsorption isotherms, displaying an IV-b type pattern, generally indicated the metal chelation process had a negligible effect on porosity of these metalloporphyrin MOFs (Fig. 1 f). The BET surface areas of PCN-224-H_2, PCN-224-Co, PCN-224-Fe, PCN-224-Cu, and PCN-224-Zn were determined to be 3906, 3466, 2943, 3993, and 3860 m^2/g, respectively. The pore size distribution calculated by nonlocalized density functional theory (NLDFT) showed all of the MOFs had micropores of 1.5 nm and mesopores of 2.4 nm (Fig. S3, Text S4). The experimental PXRD patterns of as-synthesized PCN-224-M closely matched the simulated patterns derived from X-ray single crystal structure of PCN-224, providing strong evidence of the phase purity of these MOFs (Fig. 1 g).

3.2. Photobleaching deactivation of porphyrin MOFs in advance oxidation process

Based on the analysis of the band structures (Text S4, Fig. S4) [53–55], we predicted that all PCN-224-M (M=H_2, Co, Cu, Fe, Zn) possess the capability to photocatalytically generate hydroxyl radicals from H_2O_2 under light irradiation (Text S5, Fig. S5), indicating their potential for application in advanced oxidation processes (AOPs). The results of model reactions investigating the degradation of RhB in the presence of H_2O_2 and porphyrin MOFs partially supported our prediction. In dark condition, only PCN-224-Fe and PCN-224-Co exhibited superior efficiencies in RhB degradation, while the concentration of RhB remained above 90% after 2 h when other porphyrin MOFs were used as catalysts (Fig. S6). In contrast, visible light significantly enhanced the degradation efficiencies of RhB (Fig. 2a), following a trend of PCN-224-Fe ≈ PCN-224-Co > PCN-224-H_2 > PCN-224-Cu ≈ PCN-224-Zn in the first 20 min, similar to the case under the dark. However, intriguingly, the degradation efficiency achieved by PCN-224-H_2 surpassed that of both PCN-224-Fe and PCN-224-Co after 20-min irradiation (Fig. 2a). In the initial stage, the sharply decreasing concentration of RhB when using Fe- and Co-chelated porphyrin MOFs reflected their high activity in contaminant degradation in the presence of H_2O_2. Then it became evident that their activity was not sustainable over the long term, indicating a deactivation of the catalysts. The deactivations might be related to the photobleaching phenomena of PCN-224-M, which were supported by the observation that both the colors of RhB and PCN-224-M faded when the visible irradiation was prolonged (Fig. S7). Moreover, neither the colors nor catalytic activities of photobleached PCN-224-M could be recovered by adding reductant like citric acid, indicating the irreversible nature of the deactivation (Fig. S8).

The photobleaching deactivation processes of the porphyrin MOFs were elucidated by the relative contents of porphyrin linkers in the MOFs, which was quantified by an external standard method based on the UV-Vis absorbance of Soret-band of freebase porphyrin or metalloporphyrin (Fig. S9–13). In dark conditions, PCN-224-H_2, PCN-224-Cu,

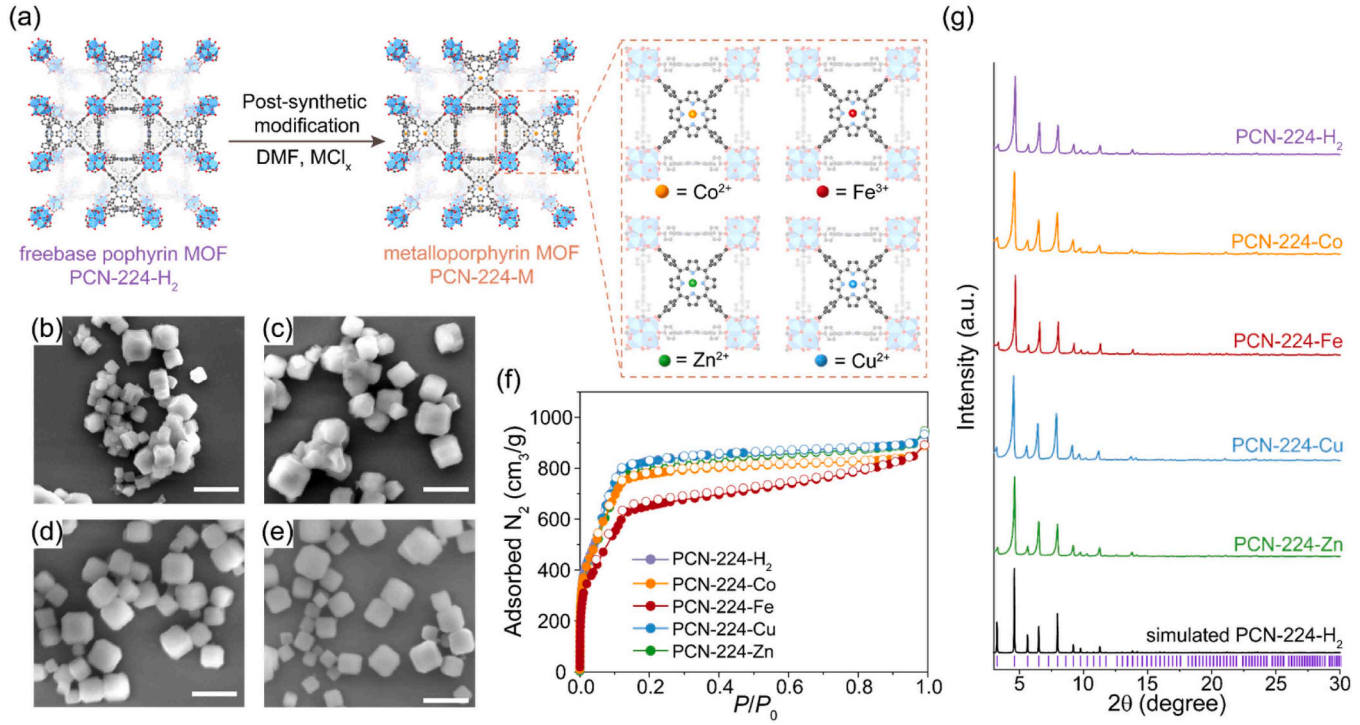

Fig. 1. (a) post-synthetic metallization of PCN-224; (b–e) SEM of PCN-224-Co (b), PCN-224-Fe (c), PCN-224-Cu (d), and PCN-224-Zn (e) (scale bar: 1 μm); (f) PXRD of PCN-224-M.

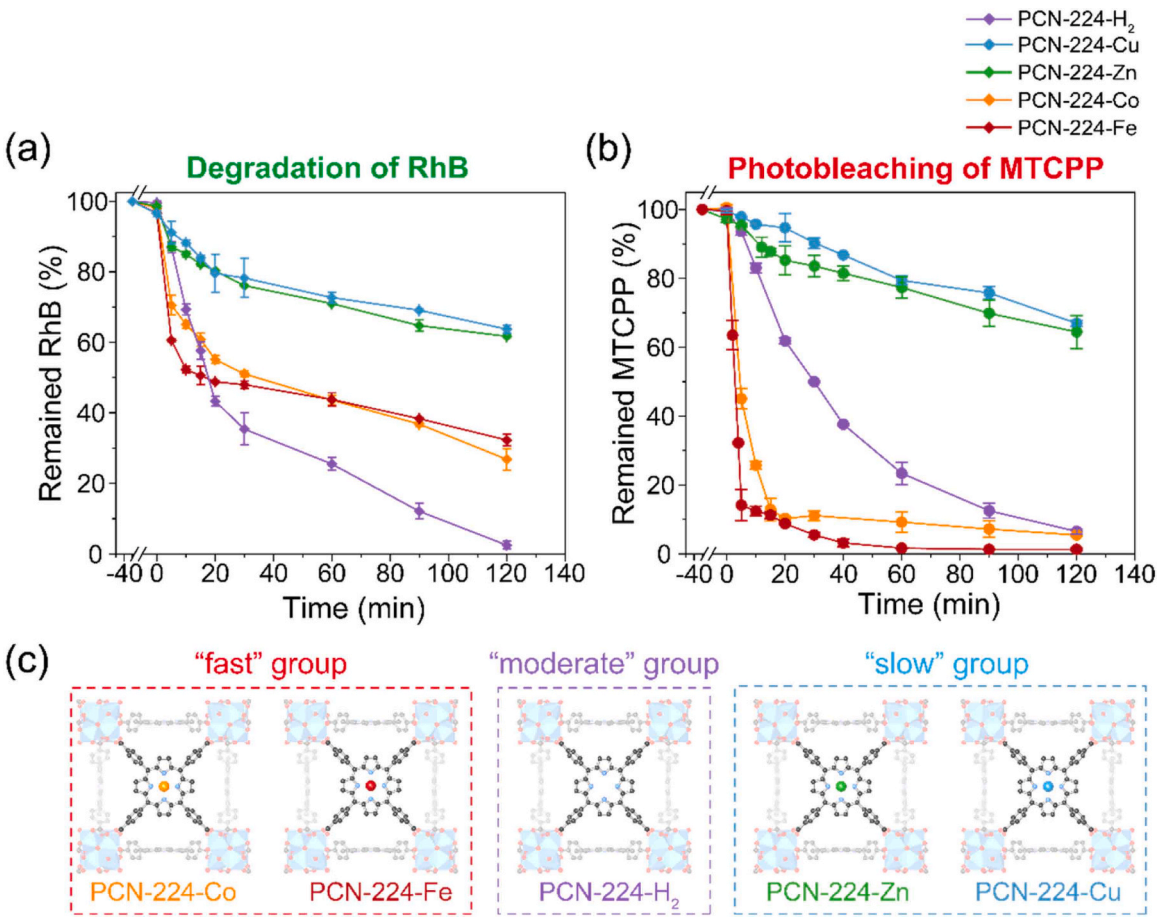

Fig. 2. Photobleaching deactivation of PCN-224-M in AOP scenario: (a) degradation efficiency of RhB using PCN-224-M catalysts under light irradiation; (b) photobleaching of PCN-224-M under light irradiation; (c) the illustration of "fast", "moderate" and "slow" photobleaching groups. The concentrations of PCN-224-M, H_2O_2, and RhB were 50 mg/L, 20 mmol/L, and 10 mg/L, respectively.

and PCN-224-Zn demonstrated comparable stability in the presence of H_2O_2, while PCN-224-Co and PCN-224-Fe underwent a bleaching process (Fig. S14). Under light irradiation, the photobleaching of porphyrin MOFs was significantly facilitated. Over 90% of CoTCPP in PCN-224-Co was bleached within only 20 min. In contrast, PCN-224-H_2 required about 120-min irradiation to achieve a similar bleaching efficiency (Fig. 2b). PCN-224-Cu and PCN-224-Zn also experienced considerable photobleaching after a 2-hour photobleaching process, with 33.1% and 35.5% of the relative porphyrin declining, respectively.

For quantitative comparison, kinetic models were employed to describe the photobleaching deactivation process of porphyrin MOFs in H_2O_2 solutions, specifically a pseudo-first-order model because of the excessive and relatively unchanged dosage of H_2O_2 (Fig. S15). The linear fitting curves and relevant parameters are listed in Fig. S16-S20. The photobleaching rate constants of PCN-224-Fe ($k = 0.21\ min^{-1}$) and PCN-224-Co ($k = 0.12\ min^{-1}$) were approximately 9.1 and 4.5 times higher than that of PCN-224-H_2 ($k = 0.023\ min^{-1}$), and significantly higher than those of PCN-224-Cu ($k = 3.3 \times 10^{-3}\ min^{-1}$) and PCN-224-Zn ($k = 3.2 \times 10^{-3}\ min^{-1}$), indicating the rapid photobleaching deactivation process of PCN-224-Fe and PCN-224-Co in H_2O_2 solution. Quantitatively, the stability against photobleaching in the presence of H_2O_2 followed the sequence: PCN-224-Fe < PCN-224-Co < < PCN-224-H_2 < PCN-224-Zn ≈ PCN-224-Cu. For the sake of convenience in the following discussion, these porphyrin MOFs were classified into three distinct categories: "fast" (PCN-224-Co and PCN-224-Fe), "moderate" (PCN-224-H_2), and "slow" (PCN-224-Cu, PCN-224-Zn) photobleaching deactivation groups (Fig. 2c).

3.3. Photochemical transformation led to the deactivation of porphyrin MOFs in H_2O_2 solution

Further structural characterizations of porphyrin MOFs illustrated photochemical transformation modes that were possible to cause the deactivation of PCN-224-M at various perspectives. The PXRD patterns of the solid residuals after a 2-hour photobleaching process did not show any characteristic peaks of PCN-224 (Fig. 3a). These results indicated that the crystal structures of PCN-224 had collapsed, even for PCN-224-Cu and PCN-224-Zn, in which 66.9% of CuTCPP and 64.5% of ZnTCPP still remained. Additionally, SEM images revealed that the particle size persisted after photobleaching process (Fig. 3b). The cubic morphology also persisted for "moderate" and "slow" photobleaching group (PCN-224-H_2, PCN-224-Cu, and PCN-224-Zn), but it was damaged for the "fast" group (Fig. 3b, S21). These results revealed the amorphization occurred during photobleaching process, especially for the "fast" photobleaching groups.

The persistence of PCN-224-M particles could be owing to the insolubility of Zr(IV), which is recognized as structural metal component in the secondary-building-units (SBUs) of PCN-224-M, in the acid and neutral aqueous solutions. This deduction was also supported by the HAADF-STEM and EDS mapping images. After light irradiation in the presence of H_2O_2, a sharp decline for the chelating metals (Co, Figs. 3c and 3d; Fe, Fig. S22) was observed for the "fast" photobleaching group, while there was a slight decrease in Cu and Zn content (Figs. 3e, 3f and S23). However, the EDS results implied different scenario for Zr in the PCN-224-M (Fig. S22–S25). This disparity was further quantified by ICP-OES. The release ratio of Zr from freebase- and metalloporphyrin MOFs

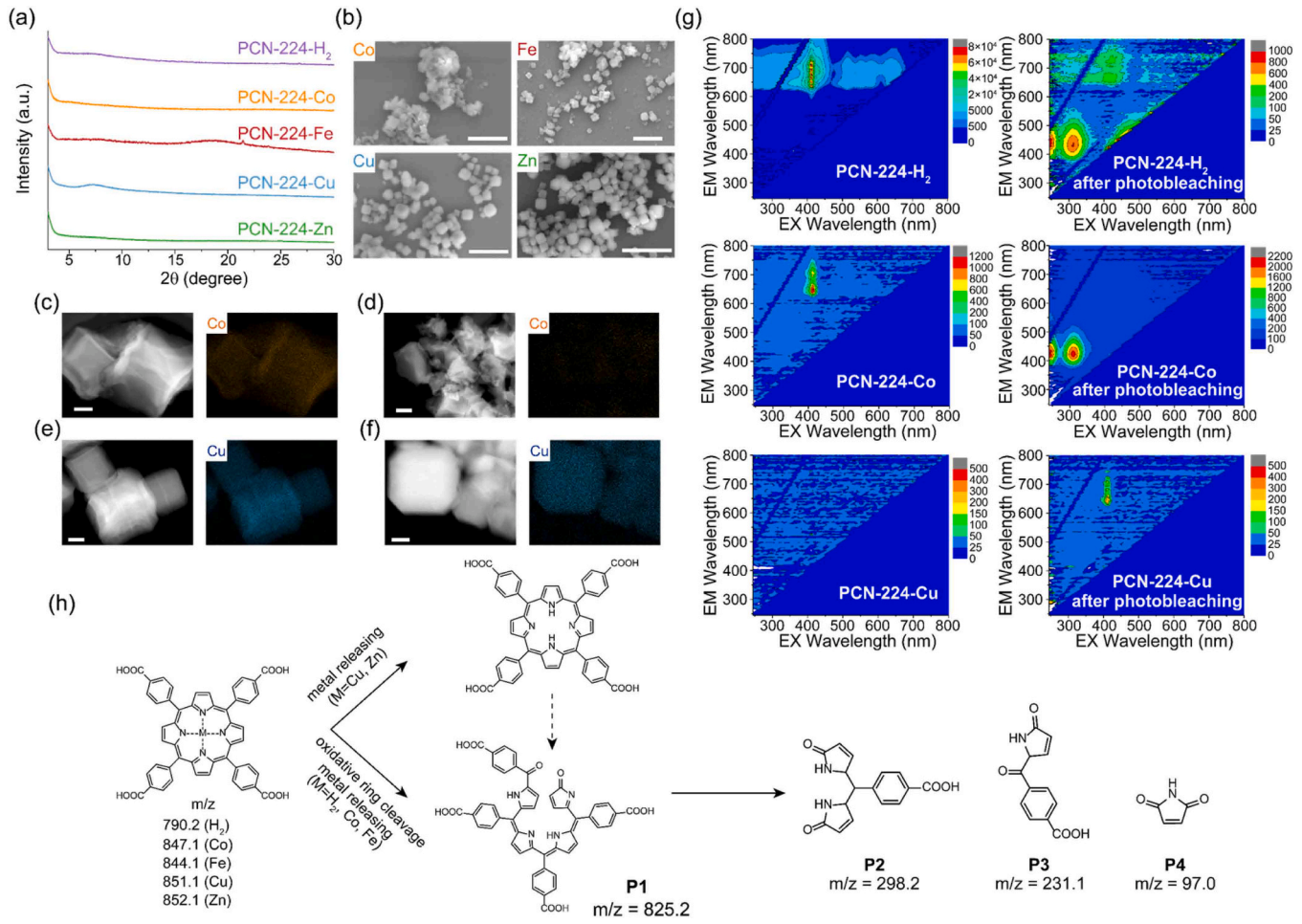

Fig. 3. Photochemical transformation of PCN-224-M in H_2O_2: (a) PXRD patterns of remained solid after 2 h exposure to visible light; (b) SEM images of metalloporphyrin MOFs (PCN-224-M, M=Co, Fe, Cu, and Zn) after 2 h irradiation (scale bar: 2 μm); (c–f) the HAADF-STEM and EDS mapping images of PCN-224-Co before light irradiation (c), PCN-224-Co after 2 h exposure to visible light (d), PCN-224-Cu before light irradiation (e), PCN-224-Cu after 2 h exposure to visible light (f); (g) EEM spectra of H_2TCPP in PCN-224-H_2, CoTCPP in PCN-224-Co, and CuTCPP in PCN-224-Cu before and after 1 h of photobleaching; (h) oxidative degradation pathway of MTCPP moieties in porphyrin MOFs.

into the supernatant solution was below 0.15%, even after 2-h photobleaching that completely destroyed the crystallinity of the MOF (Fig. S26). In contrast, the chelated metal ions were more prone to release from MOF skeleton into supernatant solution, with release ratios of 99.8%, 99.2%, 7.6%, and 18.6% for Fe, Co, Cu, and Zn, respectively (Fig. S26).

The release of metal ions chelated on porphyrin linkers is potentially associated with the cleavage of the porphyrin linkers, which deserves particular attention. Here, we selected PCN-224-H_2, PCN-224-Co, and PCN-224-Cu as representatives for "moderate", "fast", and "slow" group, respectively, to elucidate whether transformation of porphyrin linker occurred during photobleaching deactivation. The excitation-emission matrix spectra (EEM) were employed to track the transformation of fluorescent properties of organic moieties in porphyrin MOFs before and after the photobleaching process in H_2O_2 solution. Fig. 3g depicts the EEM of organic moieties in PCN-224-H_2 before and after the photobleaching process. Before the photobleaching, the fluorescence in the region of λ_{ex}-λ_{em}= (390–420 nm)-(600–700 nm) could be ascribed to the porphyrin linker H_2TCPP. After 60-min photobleaching process, the intensity of H_2TCPP region declined, and new peaks at λ_{ex}-λ_{em}= 310 nm-425 nm and 243–430 nm emerged. These red shifts in both excitation and emission peaks indicated the destruction of aromatic porphyrin ring. Notably, in the case of PCN-224-Co, the peak of Co-porphyrin (λ_{ex}-λ_{em}=420 nm-640 nm) completely disappeared within 60 min (Fig. 3g), and the peak corresponding to destructed porphyrin emerged. Conversely, in the case of PCN-224-Cu, no signal was observed in the region of porphyrin, which corresponded to fluorescent "turn-off" response between porphyrin sites and the chelated Cu(II) ions [56]. Furthermore, no peaks corresponding to destructed porphyrin at λ_{ex}-λ_{em} = 310 nm-425 nm and 243–430 nm were observed after one-hour irradiation in H_2O_2 solution, underscoring the high stability of PCN-224-Cu against destruction of aromatic porphyrin ring. However, the peak of porphyrin region emerged after photobleaching, which was corroborated with the minor percentage of Cu(II) leaching observed in the photobleaching process (Fig. S26). These results provided evidence of the cleavage of aromatic porphyrin ring of "fast" and "moderate" groups, and the release of metals from PCN-224-Cu in the "slow" group was also observed during the photobleaching process.

The decomposition of aromatic porphyrin ring during the photobleaching process was further confirmed by intermediate determining using ESI-MS (Fig. S27). In general, the identification of ring-opening products and the smaller molecules allowed for the proposal of a degradation pathway of porphyrin MOFs (Fig. 3h). Initially, the H_2TCPP linker in PCN-224 underwent a ring-cleavage oxidation at the *meso*-position to form the bilinone-like intermediate **P1** (m/z = 825.2) [57, 58]. At this stage, chelated Co^{2+} leached from porphyrin moieties in MOF structure of PCN-224-Co. Subsequently, the intermediate was further decomposed to dipyrroles **P2** (m/z = 298.1), monopyrroles **P3, P4** (m/z = 231.1, 97.0), ultimately being released from the MOF skeletons. In summary, we observed complex transformation modes of

PCN-224-M, including amorphization, chelated metal leaching, in the presence of H_2O_2 under visible light. More importantly, cleavage of porphyrin linkers was characterized, which could contribute to the reduction of the linker's rigidity and the disruption of the link arrangement periodicity.

3.4. The species result in the photobleaching deactivation of porphyrin MOFs

Ascertaining the exact species that caused ring-opening reaction of porphyrin linkers is essential for the mechanism study. On the one hand, porphyrin-based MOFs and their derivatives are able to generate ROS such as hydroxyl radical (·OH), superoxide ($O_2^{\cdot-}$), and singlet oxygen (Fig. 4a–c) [29–33]. Nevertheless, H_2O_2 itself also exhibits high oxidation activity. Therefore, a series of analysis were conducted to identify the primary factor leading to the destruction of the porphyrin linkers.

EPR spectroscopy using DMPO as a trapping agent was utilized to detect the presence of·OH radicals. It is worth noting that no significant signals were observed in the control experiments, whether in the absence of H_2O_2 or without porphyrin MOFs, under both dark and visible light irradiation conditions (Fig. S28). As a comparison, in EPR measurements involving both H_2O_2 and porphyrin MOFs (Fig. 4a), clear quartet signals with an intensity ratio of 1:2:2:1 (DMPO-OH) were observed in dark condition. The other weak signals were attributed to oxidized DMPO. These results revealed that all of the porphyrin MOFs had the ability to generate·OH in the dark. However, once visible light was introduced, the characteristic signals of·OH sharply declined. These observations brought up the hypothesis that·OH was not the main factor that caused ring-opening of porphyrin linkers in PCN-224-M, especially in the light-irradiating condition. This hypothesis was supported by the radical quenching experiments. The addition of TBA, known as·OH scavenger, did not significantly inhibit the photobleaching rate of porphyrin MOFs (Fig. 4d, Fig. S29).

The EPR signals of $O_2^{\cdot-}$ generated by PCN-224-M slightly increased after light irradiation (Fig. 4b). However, the addition of $O_2^{\cdot-}$ scavenger still could not inhibit the photodegradation of porphyrin MOFs (Fig. 4d, Fig. S30). Furthermore, PCN-224-H_2 and PCN-224-Fe could generate $^1O_2$ under light irradiation (Fig. 4c). For these two MOFs, the addition of DPBF, a scavenger of $^1O_2$ could only slightly decrease the photobleaching rate of PCN-224-H_2 and PCN-224-Fe to 0.016 min^{-1} (versus

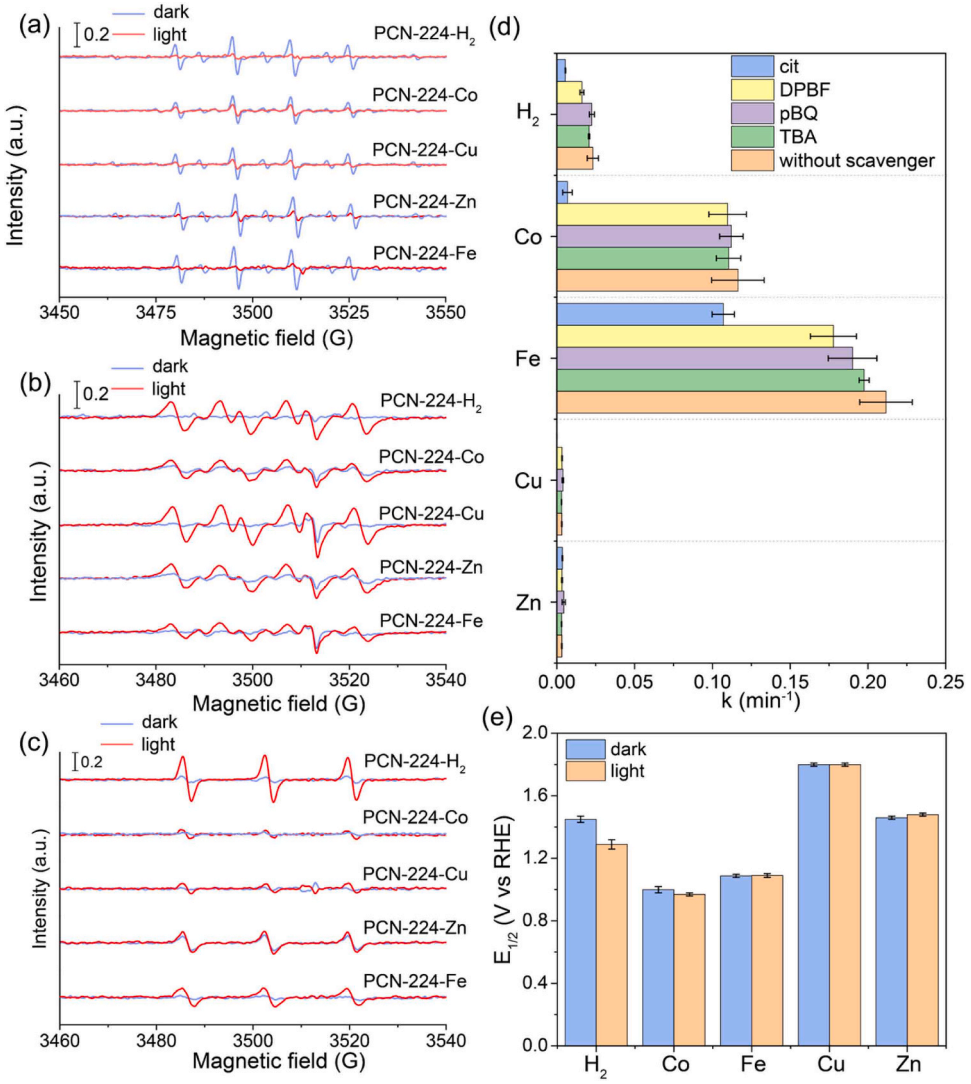

Fig. 4. Investigation of primary factor responsible for porphyrin MOFs bleaching in the presence of H_2O_2: (a) EPR spectra of PCN-224-M in aqueous solution with DMPO as radical trap, blue and red lines represent EPR spectra in dark and under light irradiation, respectively; (b) EPR spectra of PCN-224-M in MeOH solution with DMPO as radical trap; (c) the EPR spectra of PCN-224-M with TEMP as radical trap; (d) delaying effect of hydroxyl radical scavenger (TBA), superoxide scavenger (*p*-BQ), singlet oxygen scavenger (DPBF), and electron donor (citrate) for photobleaching reaction of PCN-224-M; (e) oxidation potentials of PCN-224-M under light irradiation.

0.023 min^{-1}) and 0.178 min^{-1} (versus 0.212 min^{-1}), respectively (Fig. S31). Therefore, while $^1O_2$ could contribute to the photobleaching of porphyrin MOFs, it was not the major factor.

We observed that the addition of reducing agent citrate resulted in a decrease in the photobleaching rate constants k of PCN-224-H_2, PCN-224-Co, PCN-224-Fe, PCN-224-Cu, and PCN-224-Zn to 5.4×10^{-3} min^{-1} (compared to 0.023 min^{-1} without citrate), 0.068 min^{-1} (compared to 0.11 min^{-1} without citrate), 0.10 min^{-1} ($k = 0.21$ min^{-1} without citrate) 2.5×10^{-5} min^{-1} (compared to 3.3×10^{-3} min^{-1} without citrate), and 3.5×10^{-4} min^{-1} (compared to 3.2×10^{-3} min^{-1} without citrate), respectively (Fig. 4d, Fig. S32). This significant reduction in the photobleaching by reducing agent citrate, coupled with the limited impact of ROS on the stability of metalloporphyrin MOFs, suggested that a direct reduction-oxidation (redox) reaction may occur between the porphyrin MOFs and H_2O_2 during the photobleaching process in presence of H_2O_2, instead of oxidation by the generated radicals.

3.5. Mechanisms underlying the photobleaching deactivation rates of PCN-224-M

Another intriguing aspect was the underlying mechanism governing the observation that the photobleaching deactivation behaviors of porphyrin MOFs were contingent upon the functional groups in PCN-224-M, i.e., the chelated metal ions on the porphyrin ring. This phenomenon was conveniently termed as “group effect” in the subsequent discussion. The variations in photobleaching rates among different metalloporphyrin MOFs appear to be related to their activity in redox reaction with H_2O_2. This relationship was supported by the consistency of photobleaching rates of the porphyrin MOFs and their oxidation potential E_{ox} (Fig. 4e, Fig. S33, Table S3). The “fast” photobleaching group, which include PCN-224-Co and PCN-224-Fe, exhibits low E_{ox} values at 0.97 V and 1.09 V versus RHE, respectively. Similarly, the “moderate” photobleaching group (PCN-224-H_2, E_{ox} at 1.29 V) and “slow” photobleaching group (PCN-224-Zn, E_{ox} at 1.48 V; PCN-224-Cu, E_{ox} at 1.79 V) follow this pattern. While the E_{ox} values of PCN-224-M do correlate strongly with their photobleaching rates, there are still observable differences in the redox potentials of PCN-224-M that warrant further investigation into the mechanism.

We postulated that the “group effect” could be attributed to the different capacities of distinct porphyrin functional groups to form a reactive metal-oxo-porphyrin intermediate. This hypothesis was inspired by the reported works in the field of biological and biomimetic catalysis. In typical catalytic process involving heme-based peroxidases, the iron(III)-porphyrin sites are firstly oxidized to form iron(IV)-oxo-porphyrin-based π-free radicals with high reactivity (referred to as compound I, Fig. S34) [59,60]. “Suicide inactivation” occurs if compound I is partly reduced by an electron donor within the protein structure through one-electron pathway, resulting in the formation of iron(IV)-oxo-porphyrin (compound II). When H_2O_2 is added, it forms HOO··iron(III) porphyrin intermediate (compound III), which then undergoes irreversible ring-opening bleaching and further degradation (Fig. S35) [61]. A similar process might also be involved in the bleaching of porphyrin MOFs.

Based on this hypothesis, it can be deduced that the formation of M-oxo-porphyrin intermediate and the partial reduction of this intermediate are two crucial factors. Therefore, a specific metalloporphyrin linker in PCN-224-M could possibly react with H_2O_2 to form reactive oxo-metal porphyrin intermediate (Fig. S34a); if this intermediate was partly reduced by another electron donor to form M-oxo-porphyrin (Fig. S34b), this porphyrin site became more susceptible to further bleaching and degradation processes.

Notably, the formation of M-oxo-porphyrin intermediate is the first step of bleaching process, and the differences in stability are determined by whether the MOF can engage with H_2O_2 to form this crucial intermediate. In this regard, ESI-MS analysis of the reactions between PCN-224-Co and PCN-224-Cu with H_2O_2 was performed as representatives [62]. The MOFs were dissolved in NaOH solutions to release linkers and then diluted by ultrapure water before the measurements. Fig. 5a showed the mass spectra of dissolved PCN-224-Co exposed to H_2O_2 for a mere 15 s, which revealed a prominent signal at $m/z = 881.12$ corresponding to the CoTCPP linker bonded with an H_2O_2 molecule. In contrast, Fig. 5b demonstrates a notably weaker signal of $[TCPPCu\text{-}H_2O_2]^+$ ($m/z = 886.13$), indicating the greater difficulty of Cu-chelated porphyrin linkers to interact with H_2O_2 molecules compared to Co-chelated counterparts. Further immersion of the metalloporphyrin MOFs in H_2O_2 solution for 300 s resulted in the detection of the $[TCPPCo\text{-}O]^+$ fragment ($m/z = 863.12$). However, even with extended reaction time, no signal for $[TCPPCu\text{-}O]^+$ fragment emerged. This finding highlights the rapid formation of Co-oxo-porphyrin intermediate [63], and the relative inert nature of CuTCPP linkers in both H_2O_2 interaction and Cu-oxo porphyrin intermediate formation in PCN-224-Cu.

DFT calculations were employed in conjunction with the experimental results to elucidate the structure-stability relationships of PCN-224-M in the presence of H_2O_2 (Text S6, Fig. S36). Specifically, PCN-224-Ni and PCN-224-Mn were included to further establish the structure-stability relationships of PCN-224-Ms (Fig. S37). The experimental findings demonstrated photobleaching rates of 0.183 min^{-1} for PCN-224-Mn and 3.2×10^{-3} min^{-1} for PCN-224-Ni (Fig. S37), thereby categorizing PCN-224-Mn and PCN-224-Ni as "fast" and "slow" bleaching groups, respectively. Through DFT calculations, the free energy (ΔG) in the adsorption step of H_2O_2 and the formation of metal-oxo-porphyrin were simulated (Fig. 5e). In the absence of metal sites, freebase-porphyrin exhibited a lower H_2O_2 binding energy (0.02 eV) compared to metalloporphyrin (0.26–2.98 eV) (Fig. S38). As for the metalloporphyrin, the photobleaching rate of PCN-224-M (log k) was negatively correlated with the ΔG value of M-oxo-porphyrin formation (Fig. 5f). Specifically, the ΔG value of “fast group” (PCN-224-M, M=Fe, Mn, Co) was negative, meaning that the formation of the M-oxo-porphyrin intermediate was theoretically spontaneous and thus experience faster photobleaching deactivation (red area, Fig. 5f). This observation can be attributed to the electronic structures of the chelated metal ions. In the case of the "fast" group, the metal 3d orbitals either constituted the highest occupied molecular orbitals (HOMO) (M=Fe, Mn) or were in close proximity to the HOMO (M=Co) as indicated by the density-of-states (DOS) analysis (Fig. S39), suggesting that direct electron removal from the metal or metal-ligand electron transfer were prone to occur during oxidation [64–67]. Consequently, the chelation of Mn, Fe, or Co ions facilitated the oxidation of the corresponding porphyrin linkers, resulting in the formation of M-oxo-porphyrin. On the other hand, given that the chelated metals in PCN-224-M (M=Cu, Zn, Ni) were significantly distant from the HOMO of metalloporphyrin, and the formation of the intermediate was more challenging, i.e., the ΔG value was positive, they displayed a greater stability against photobleaching deactivation (blue area, Fig. 5f).

Collectively, we propose a comprehensive photobleaching deactivation mechanism of PCN-224-M in H_2O_2 solution (Fig. 6). PCN-224-Fe, PCN-224-Mn, and PCN-224-Co and can form the Mn(IV)-oxo, Fe(IV)-oxo-, and Co(IV)-oxo-porphyrins, making them susceptible to bleaching deactivation even in dark conditions. Under light irradiation, the excitons at metalloporphyrin sites in the MOFs can efficiently migrate to new sites by strut-to-strut intercomponent energy transfer (EnT) [68,69], or center metal redox hopping [70]. If one of the metalloporphyrin linkers form M-oxo-porphyrin intermediate, it can be partly reduced by the photo-excited electrons generated from the adjacent porphyrin/metalloporphyrin linker and transform to an unstable structure in the presence of H_2O_2. This transformation pathway enables visible light to significantly accelerate the bleaching process of PCN-224-Co and PCN-224-Fe. Freebase porphyrin linker H_2TCPP in PCN-224-H_2 can directly react with H_2O_2 under light irradiation, although DFT calculations indicate the weaker interaction between H_2O_2 and

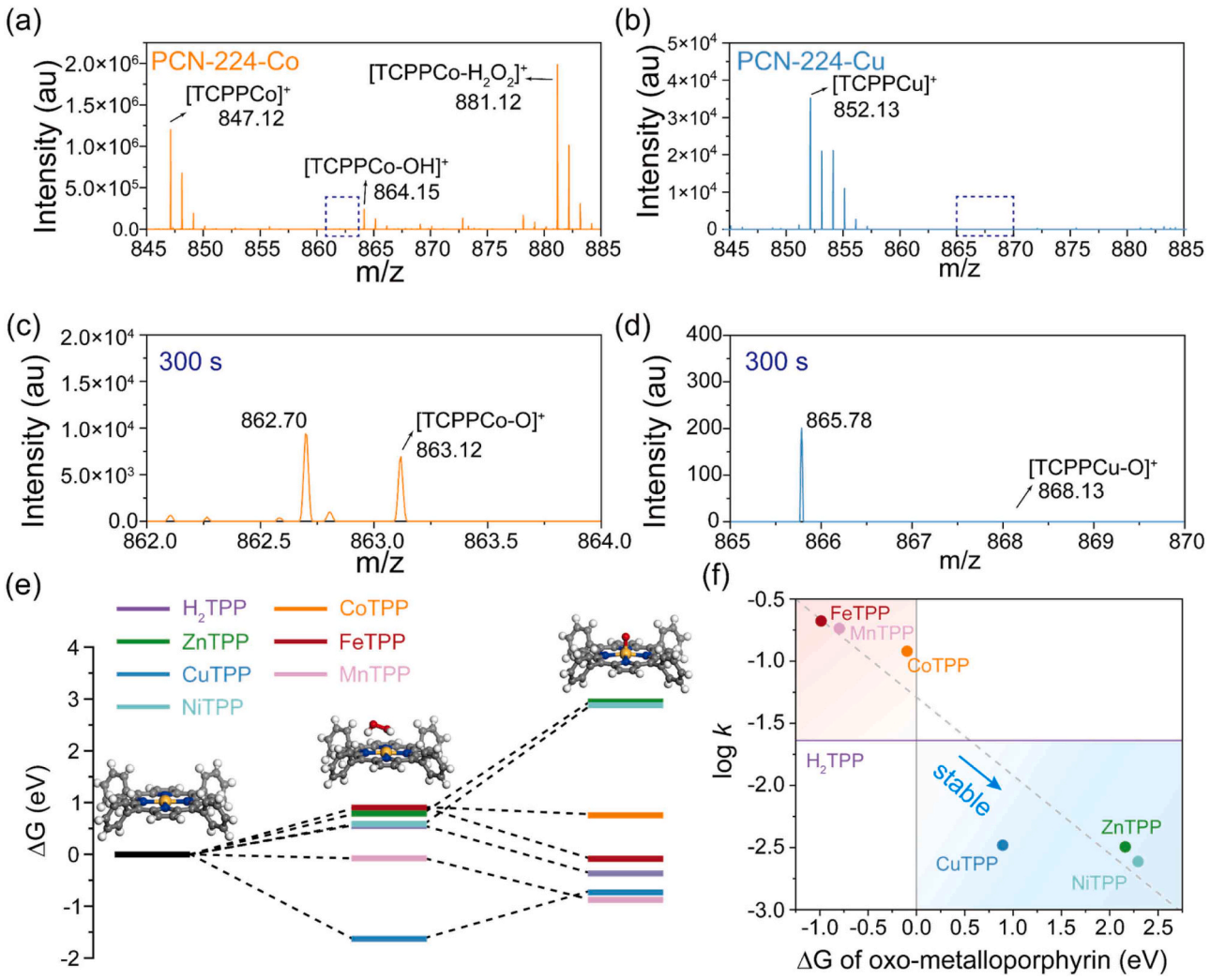

Fig. 5. Demonstration of oxo-metal-porphyrin intermediates: (a, b) ESI-MS analysis of the reaction between H_2O_2 and metalloporphyrin MOFs PCN-224-Co (a), and PCN-224-Cu (b), the dash rectangle marked the areas where $[TCPPM\text{-}O]^+$ might emerge; (c, d) ESI-MS results at the *m/z* area of adduct of CoTCPP (c), and PCN-224-Cu (d) with O atom reacted for 300 s; (e) free energy schemes (298 K) for reaction of PCN-224-M with H_2O_2 from DFT calculations; (f) The logarithm of photobleaching rate constant values (log *k*) of PCN-224-M versus the ΔG of oxo-metalloporphyrin formation.

freebase-porphyrin linkers. Consequently, PCN-224-H_2 undergoes a photobleaching in H_2O_2 solution with a moderate reaction rate. As for the PCN-224-Cu and PCN-224-Zn, although they were hard to form the M-oxo-porphyrin intermediate, slow photobleaching processes could be still observed under light irradiation in H_2O_2 solution. We speculated that the slow photobleaching of them was related to the central metal releasing and further redox reaction between the formed freebase porphyrin linkers and H_2O_2.

4. Conclusion

In this study, we conducted comprehensive investigation into the photobleaching deactivation of porphyrin MOFs PCN-224-M in the presence of H_2O_2. Under light irradiation, all of the porphyrin MOFs exhibited varying degrees of accelerated photobleaching. Furthermore, we observed the "group effect", which categorized the porphyrin MOFs into fast, moderate, and slow photobleaching groups based on their porphyrin functional groups: PCN-224-Fe ≈ PCN-224-Co < < PCN-224-H_2 < PCN-224-Zn ≈ PCN-224-Cu. Through the utilization of combined characterization techniques, we identified several transformation modes, including amorphization, crystallinity destruction, and demetallation. More importantly, cleavage of porphyrin linkers was characterized, which could contribute to the reduction of the linker's rigidity and cause the loss of M-N_4 active sites. Additionally, we discussed the mechanisms underlying photobleaching and found that the photobleaching of freebase and metalloporphyrin MOFs occurred due to direct redox reactions with H_2O_2. The influence of functional groups on the photobleaching behavior of the PCN-224-M was also unveiled. The electronic structures and formation of metal-oxo-porphyrin intermediates played a pivotal role in determining the photobleaching rate and stability of the porphyrin MOFs. We anticipate this study could provide a molecular-level insights into the structure-stability relationships of MOFs in the AOP scenarios.

Moreover, the cycling stabilities of MOFs and MOF-based materials have gained prominence due to their extensive study and application in chemical and physical water treatment. Therefore, future research should focus on investigating the transformation of other MOF-based catalysts. This will facilitate the design and modification of catalysts with exceptional efficiency and high stability. Building upon the demonstration of the transformation process and underlying mechanism, we propose the following suggestions to improve the sustainability of photocatalytic activity: 1) enhancing the rigidity of the linker by expanding the aromatic rings or replacing with more stable porphyrin-like M-N_4 structures; 2) impeding the migration of excitons under light irradiation by modifying the SBUs of the porphyrin MOFs, and 3) stabilizing the metal-oxo active intermediates modifying the functional

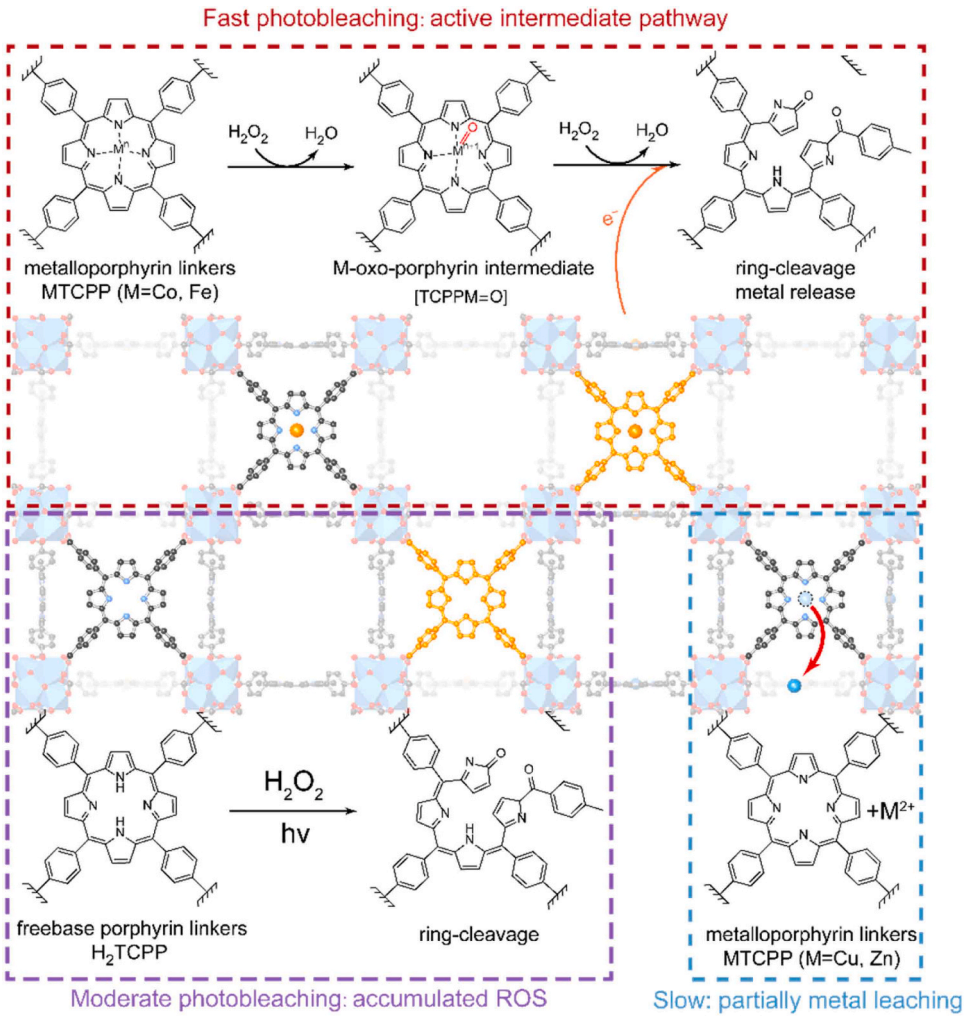

Fig. 6. The schematic illustration of proposed mechanism.

groups on porphyrin linkers. By implementing these ideas, it is possible to enhance the sustainability and efficiency of photocatalytic activity in MOFs.

CRediT authorship contribution statement

Liu Bei: Formal analysis, Methodology, Writing – review & editing. **Zhang Meng:** Formal analysis, Methodology. **Wang Zhongying:** Conceptualization, Funding acquisition, Supervision, Writing – review & editing. **Liu Xun:** Data curation, Methodology. **Shu Yufei:** Data curation, Investigation, Methodology, Writing – original draft.

Declaration of Competing Interest

The authors declare that they have no known competing financial interests or personal relationships that could have appeared to influence the work reported in this paper.

Data Availability

Data will be made available on request.

Acknowledgements

This research was supported by the National Natural Science Foundation of China (No. 22076075) and the Key Program of Fundamental Research from the Shenzhen Science and Technology Innovation Commission (No. JCYJ20220818100218039). The authors acknowledge the assistance of SUSTech Core Research Facilities.

Appendix A. Supporting information

Supplementary data associated with this article can be found in the online version at doi:10.1016/j.apcatb.2024.123746.

References

[1] S. He, Y. Chen, X. Li, L. Zeng, M. Zhu, Heterogeneous photocatalytic activation of persulfate for the removal of organic contaminants in water: a critical review, ACS EST Eng. 2 (2022) 527–546.
[2] H. Liu, C. Wang, G. Wang, Photocatalytic advanced oxidation processes for water treatment: recent advances and perspective, Chem. – Asian J. 15 (2020) 3239–3253.
[3] S.K. Loeb, P.J.J. Alvarez, J.A. Brame, E.L. Cates, W. Choi, J. Crittenden, D. D. Dionysiou, Q. Li, G. Li-Puma, X. Quan, D.L. Sedlak, T. David Waite, P. Westerhoff, J.-H. Kim, The technology horizon for photocatalytic water treatment: sunrise or sunset? Environ. Sci. Technol. 53 (2019) 2937–2947.
[4] M.N. Chong, B. Jin, C.W.K. Chow, C. Saint, Recent developments in photocatalytic water treatment technology: a review, Water Res. 44 (2010) 2997–3027.
[5] P. Singh, B. Mohan, V. Madaan, R. Ranga, P. Kumari, S. Kumar, V. Bhankar, P. Kumar, K. Kumar, Nanomaterials photocatalytic activities for waste water treatment: a review, Environ. Sci. Pollut. Res. 29 (2022) 69294–69326.
[6] A. Saravanan, P.S. Kumar, S. Jeevanantham, M. Anubha, S. Jayashree, Degradation of toxic agrochemicals and pharmaceutical pollutants: Effective and alternative approaches toward photocatalysis, Environ. Pollut. 298 (2022) 118844.

[7] A. Serrà, L. Philippe, F. Perreault, S. Garcia-Segura, Photocatalytic treatment of natural waters. Reality or hype? The case of cyanotoxins remediation, Water Res. 188 (2021) 116543.

[8] Introduction to Metal–Organic Frameworks, Chemical Reviews, 112 (2012) 673–674.

[9] G. Cai, P. Yan, L. Zhang, H.-C. Zhou, H.-L. Jiang, Metal–organic framework-based hierarchically porous materials: synthesis and applications, Chem. Rev. 121 (2021) 12278–12326.

[10] H. Li, M. Eddaoudi, M. O'Keeffe, O.M. Yaghi, Design and synthesis of an exceptionally stable and highly porous metal-organic framework, Nature 402 (1999) 276–279.

[11] S. Chen, Z. Li, L. Wu, L. Liu, J. Hu, H. Hou, S. Liang, J. Yang, Generation of high-valent iron-oxo porphyrin cation radicals on hemin loaded carbon nanotubes for efficient degradation of sulfathiazole, J. Hazard. Mater. 444 (2023) 130402.

[12] X. Yang, P. Zhang, H. Hou, J. Hu, L. Liu, L. Wu, S. Chen, K. Pan, S. Liang, S. Yuan, J. Yang, An iron chlorophyll derivative for enhanced degradation of bisphenol A: new insight into the generation mechanism of high-valent iron oxo species, Chem. Eng. J. 451 (2023) 138688.

[13] S. Chen, J. Hu, L. Lu, L. Wu, Z. Liang, J. Tang, H. Hou, S. Liang, J. Yang, Iron porphyrin-TiO2 modulated peroxymonosulfate activation for efficient degradation of 2,4,6-trichlorophenol with high-valent iron-oxo species, Chemosphere 309 (2022) 136744.

[14] Z.-B. Fang, T.-T. Liu, J. Liu, S. Jin, X.-P. Wu, X.-Q. Gong, K. Wang, Q. Yin, T.-F. Liu, R. Cao, H.-C. Zhou, Boosting interfacial charge-transfer kinetics for efficient overall CO_2 photoreduction via rational design of coordination spheres on metal–organic frameworks, J. Am. Chem. Soc. 142 (2020) 12515–12523.

[15] Z.-Q. Li, G.-L. Zhu, R.-J. Mo, M.-Y. Wu, X.-L. Ding, L.-Q. Huang, Z.-Q. Wu, X.-H. Xia, Light-enhanced osmotic energy harvester using photoactive porphyrin metal–organic framework membranes, Angew. Chem. Int. Ed. 61 (2022) e202202698.

[16] D. Han, Y. Han, J. Li, X. Liu, K.W.K. Yeung, Y. Zheng, Z. Cui, X. Yang, Y. Liang, Z. Li, S. Zhu, X. Yuan, X. Feng, C. Yang, S. Wu, Enhanced photocatalytic activity and photothermal effects of cu-doped metal-organic frameworks for rapid treatment of bacteria-infected wounds, Appl. Catal. B: Environ. 261 (2020) 118248.

[17] K. Wang, J. Cui, L. Li, Z. Yang, S. Zeng, Z. Hu, C. Hu, Y. Zhao, Single-atom sites in metal–N4 configuration for efficient abatement of refractory organic pollutants via Fenton-like reaction, Chem. Eng. J. 476 (2023) 146622.

[18] W. Qu, M. Luo, Z. Tang, T. Zhong, H. Zhao, L. Hu, D. Xia, S. Tian, D. Shu, C. He, Accelerated catalytic ozonation in a mesoporous carbon-supported atomic Fe–N4 sites nanoreactor: confinement effect and resistance to poisoning, Environ. Sci. Technol. 57 (2023) 13205–13216.

[19] Z. Wang, Q. Li, R. Su, G. Lv, Z. Wang, B. Gao, W. Zhou, Enhanced degradation of bisphenol F in a porphyrin-MOF based visible-light system under high salinity conditions, Chem. Eng. J. 428 (2022) 132106.

[20] X.-H. Chen, Y.-S. Zhang, W.-B. Li, X.-W. Guan, J.-W. Ye, L. Chen, H.-P. Wang, J. Bai, Z.-W. Mo, X.-M. Chen, A porphyrin-based metal–organic framework with highly efficient adsorption and photocatalytic degradation performances for organic dyes, Inorg. Chem. Front. 9 (2022) 2328–2335.

[21] J. Liu, W.H. Xiong, L.Y. Ye, W.S. Zhang, H. Yang, Developing a novel nanoscale porphyrinic metal–organic framework: a bifunctional platform with sensitive fluorescent detection and elimination of nitenpyram in agricultural environment, J. Agric. Food Chem. 68 (2020) 5572–5578.

[22] P. Zhao, J. Wang, X. Han, J. Liu, Y. Zhang, B. Van der Bruggen, Zr-porphyrin metal–organic framework-based photocatalytic self-cleaning membranes for efficient dye removal, Ind. Eng. Chem. Res. 60 (2021) 1850–1858.

[23] Z. Xia, B. Shi, W. Zhu, C. Lü, Temperature-responsive polymer-tethered Zr-porphyrin MOFs encapsulated carbon dot nanohybrids with boosted visible-light photodegradation for organic contaminants in water, Chem. Eng. J. 426 (2021) 131794.

[24] P. Jin, L. Wang, X. Ma, R. Lian, J. Huang, H. She, M. Zhang, Q. Wang, Construction of hierarchical ZnIn2S4@PCN-224 heterojunction for boosting photocatalytic performance in hydrogen production and degradation of tetracycline hydrochloride, Appl. Catal. B: Environ. 284 (2021) 119762.

[25] J. Li, X. Li, G. Wu, J. Guo, X. Yin, M. Mu, Construction of 2D Co-TCPP MOF decorated on B-TiO2−X nanosheets: Oxygen vacancy and 2D–2D heterojunctions for enhancing visible light-driven photocatalytic degradation of bisphenol A, J. Environ. Chem. Eng. 9 (2021) 106723.

[26] C. Yang, S. Shang, Y. Fan, K. Shih, X.-y Li, L. Lin, Incorporation of atomically dispersed cobalt in the 2D metal–organic framework of a lamellar membrane for highly efficient peroxymonosulfate activation, Appl. Catal. B: Environ. 325 (2023) 122344.

[27] Z.-H. Zhu, Y. Liu, C. Song, Y. Hu, G. Feng, B.Z. Tang, Porphyrin-based two-dimensional layered metal–organic framework with sono-/photocatalytic activity for water decontamination, ACS Nano 16 (2022) 1346–1357.

[28] N. Wang, S. Liu, Z. Sun, Y. Han, J. Xu, Y. Xu, J. Wu, H. Meng, B. Zhang, X. Zhang, Synergistic adsorption and photocatalytic degradation of persist synthetic dyes by capsule-like porphyrin-based MOFs, Nanotechnology 32 (2021) 465705.

[29] Y. Zhou, W. Yang, M. Qin, H. Zhao, Self-assembly of metal–organic framework thin films containing metalloporphyrin and their photocatalytic activity under visible light, Appl. Organomet. Chem. 30 (2016) 188–192.

[30] C. Qi, S. Han, J. Lin, J. Cheng, K. Du, Y. Hu, Y. Chen, Reconstruction of electronic structure of MOF-525 via metalloporphyrin for enhanced photoelectro-fenton process, Catalysts 12 (2022) 671.

[31] C.P. Yang, C.Y. Hu, Z.W. Jiang, S.Y. Xiao, X.Y. Wang, C.Z. Huang, Y.F. Li, S.J. Zhen, Facile synthesis of porphyrin-MOFs with high photo-Fenton activity to efficiently degrade ciprofloxacin, J. Colloid Interface Sci. 622 (2022) 690–699.

[32] L. Wang, P. Jin, S. Duan, J. Huang, H. She, Q. Wang, T. An, Accelerated Fenton-like kinetics by visible-light-driven catalysis over iron(iii) porphyrin functionalized zirconium MOF: effective promotion on the degradation of organic contaminants, Environ. Sci.: Nano 6 (2019) 2652–2661.

[33] W.-Q. Li, Y.-X. Wang, J.-Q. Chen, N.-N. Hou, Y.-M. Li, X.-C. Liu, R.-R. Ding, G.-N. Zhou, Q. Li, X.-G. Zhou, Y. Mu, Boosting photo-Fenton process enabled by ligand-to-cluster charge transfer excitations in iron-based metal organic framework, Appl. Catal. B: Environ. 302 (2022) 120882.

[34] L. Shi, L. Yang, H. Zhang, K. Chang, G. Zhao, T. Kako, J. Ye, Implantation of Iron (III) in porphyrinic metal organic frameworks for highly improved photocatalytic performance, Appl. Catal. B: Environ. 224 (2018) 60–68.

[35] S.H. Mehdi, D.A. Brisbin, W.A.E. McBryde, The stability of porphyrin and metalloporphyrin molecular complexes in solution, Biochimica et Biophysica Acta (BBA) - General Subjects, 444 (1976) 407–415.

[36] A.K. Sobbi, D. Wöhrle, D. Schlettwein, Photochemical stability of various porphyrins in solution and as thin film electrodes, J. Chem. Soc. Perkin Trans. 2 (1993) 481–488.

[37] G. Schnurpfeil, A.K. Sobbi, W. Spiller, H. Kliesch, D. Wöhrle, Photo-oxidative Stability and its correlation with semi-empirical MO calculations of various tetraazaporphyrin derivatives in solution, J. Porphyr. Phthalocyanines 1 (1997) 159–167.

[38] A.L. Tessaro, D.M. Fernandes, A.J. Terezo, V.R. de Souza, N. Hioka, Influences of experimental parameters on the stability of a benzoporphyrin drug in water/ethanol mixtures: a statistical approach investigation, J. Porphyr. Phthalocyanines 09 (2005) 609–616.

[39] E.F.F. da Silva, F.M. Pimenta, B.W. Pedersen, F.H. Blaikie, G.N. Bosio, T. Breitenbach, M. Westberg, M. Bregnhøj, M. Etzerodt, L.G. Arnaut, P.R. Ogilby, Intracellular singlet oxygen photosensitizers: on the road to solving the problems of sensitizer degradation, bleaching and relocalization, Integrative, Biology 8 (2016) 177–193.

[40] B. Pramanik, R. Sahoo, M.C. Das, pH-stable MOFs: Design principles and applications, Coord. Chem. Rev. 493 (2023) 215301.

[41] Z. Chen, K.O. Kirlikovali, L. Shi, O.K. Farha, Rational design of stable functional metal–organic frameworks, Mater. Horiz. (2023).

[42] K. Wang, Y. Li, L.-H. Xie, X. Li, J.-R. Li, Construction and application of base-stable MOFs: a critical review, Chem. Soc. Rev. 51 (2022) 6417–6441.

[43] M. Ding, X. Cai, H.-L. Jiang, Improving MOF stability: approaches and applications, Chem. Sci. 10 (2019) 10209–10230.

[44] L. Wang, X. Li, B. Yang, K. Xiao, H. Duan, H. Zhao, The chemical stability of metal-organic frameworks in water treatments: Fundamentals, effect of water matrix and judging methods, Chem. Eng. J. 450 (2022) 138215.

[45] D. Mateo, A. Santiago-Portillo, J. Albero, S. Navalón, M. Alvaro, H. García, Long-term photostability in terephthalate metal–organic frameworks, Angew. Chem. Int. Ed. 58 (2019) 17843–17848.

[46] W. Zheng, M. Liu, L.Y.S. Lee, Electrochemical instability of metal–organic frameworks: in situ spectroelectrochemical investigation of the real active sites, ACS Catal. 10 (2020) 81–92.

[47] M. Taheri, T. Tsuzuki, Photo-accelerated hydrolysis of metal organic framework ZIF-8, ACS Mater. Lett. 3 (2021) 255–260.

[48] C. Yue, L. Wu, Y. Lin, Y. Lu, C. Shang, R. Ma, X. Zhang, X. Wang, W.D. Wu, X. D. Chen, Z. Wu, Study on the stability, evolution of physicochemical properties, and postsynthesis of metal–organic frameworks in bubbled aqueous ozone solution, ACS Appl. Mater. Interfaces 13 (2021) 26264–26277.

[49] D. Feng, W.-C. Chung, Z. Wei, Z.-Y. Gu, H.-L. Jiang, Y.-P. Chen, D.J. Darensbourg, H.-C. Zhou, Construction of ultrastable porphyrin Zr metal–organic frameworks through linker elimination, J. Am. Chem. Soc. 135 (2013) 17105–17110.

[50] Y. Shu, Y. Chen, Q. Han, X. Liu, B. Liu, Z. Wang, Selective and light-enhanced Au (III) recovery by a porphyrin-based metal–organic framework: performance and underlying mechanisms, ACS EST Eng. 3 (2023) 1042–1052.

[51] D. Yang, S. Zuo, H. Yang, Y. Zhou, Q. Lu, X. Wang, Tailoring layer number of 2D porphyrin-based MOFs towards photocoupled electroreduction of CO_2, Adv. Mater. 34 (2022) 2107293.

[52] T. Lu, F. Chen, Multiwfn: A multifunctional wavefunction analyzer, Journal of Computational Chemistry 33 (2012) 580–592.

[53] J. Tauc, R. Grigorovici, A. Vancu, Optical properties and electronic structure of amorphous germanium, Phys. Status Solidi (B) 15 (1966) 627–637.

[54] P. Makuła, M. Pacia, W. Macyk, How to correctly determine the band gap energy of modified semiconductor photocatalysts based on UV–vis spectra, J. Phys. Chem. Lett. 9 (2018) 6814–6817.

[55] P.M. Wood, The potential diagram for oxygen at pH 7, Biochem. J. 253 (1988) 287–289.

[56] L. Li, S. Shen, R. Lin, Y. Bai, H. Liu, Rapid and specific luminescence sensing of Cu (ii) ions with a porphyrinic metal–organic framework, Chem. Commun. 53 (2017) 9986–9989.

[57] B. Evans, K.M. Smith, J.A.S. Cavaleiro, Ring cleavage of meso-tetraphenylporphyrin, Tetrahedron Lett. 17 (1976) 4863–4866.

[58] J.A.S. Cavaleiro, M.J.E. Hewlins, A.H. Jackson, G.P. Maria, S. Neves, Structures of the ring-opened oxidation products from meso-tetraphenylporphyrin, J. Chem. Soc. Chem. Commun. (1986) 142–144.

[59] P. George, Intermediate compound formation with peroxidase and strong oxidizing agents, J. Biol. Chem. 201 (1953) 413–426.

[60] H.B. Dunford, J.S. Stillman, On the function and mechanism of action of peroxidases, Coord. Chem. Rev. 19 (1976) 187–251.

[61] B. Valderrama, M. Ayala, R. Vazquez-Duhalt, Suicide inactivation of peroxidases and the challenge of engineering more robust enzymes, Chem. Biol. 9 (2002) 555–565.
[62] M. Guo, H. Dong, J. Li, B. Cheng, Y.-q Huang, Y.-q Feng, A. Lei, , Spectroscopic observation of iodosylarene metalloporphyrin adducts and manganese(V)-oxo porphyrin species in a cytochrome P450 analogue, Nature, Communications 3 (2012) 1190.
[63] N. Li, W. Lu, K. Pei, Y. Yao, W. Chen, Formation of high-valent cobalt-oxo phthalocyanine species in a cellulose matrix for eliminating organic pollutants, Appl. Catal. B: Environ. 163 (2015) 105–112.
[64] T. Lu, F. Chen, Multiwfn: a multifunctional wavefunction analyzer, J. Comput. Chem. 33 (2012) 580–592.
[65] M.-S. Liao, S. Scheiner, Electronic structure and bonding in metal porphyrins, metal=Fe, Co, Ni, Cu, Zn, J. Chem. Phys. 117 (2002) 205–219.
[66] S. Hamad, N.C. Hernandez, A. Aziz, A.R. Ruiz-Salvador, S. Calero, R. Grau-Crespo, Electronic structure of porphyrin-based metal–organic frameworks and their suitability for solar fuel production photocatalysis, J. Mater. Chem. A 3 (2015) 23458–23465.
[67] Q. Sun, Y. Dai, Y. Ma, X. Li, W. Wei, B. Huang, Two-dimensional metalloporphyrin monolayers with intriguing electronic and spintronic properties, J. Mater. Chem. C 3 (2015) 6901–6907.
[68] H.-J. Son, S. Jin, S. Patwardhan, S.J. Wezenberg, N.C. Jeong, M. So, C.E. Wilmer, A. A. Sarjeant, G.C. Schatz, R.Q. Snurr, O.K. Farha, G.P. Wiederrecht, J.T. Hupp, Light-harvesting and ultrafast energy migration in porphyrin-based metal–organic frameworks, J. Am. Chem. Soc. 135 (2013) 862–869.
[69] S.S. Rajasree, X. Li, P. Deria, Physical properties of porphyrin-based crystalline metal—organic frameworks, Communications Chemistry, 4 (2021) 47.
[70] K. Maindan, X. Li, J. Yu, P. Deria, Controlling Charge-transport in metal–organic frameworks: contribution of topological and spin-state variation on the iron–porphyrin centered redox hopping rate, J. Phys. Chem. B 123 (2019) 8814–8822.